Quantum Dot Sensitized Solar Cells. A Tale of Two Semiconductor Nanocrystals: CdSe and CdTe

Jin Ho Bang and Prashant V. Kamat*

Radiation Laboratory and Department of Chemistry and Biochemistry, University of Notre Dame, Notre Dame, Indiana 46556

ARTICLE

ABSTRACT CdSe and CdTe nanocrystals are linked to nanostructured TiO_2 films using 3-mercaptopropionic acid as a linker molecule for establishing the mechanistic aspects of interfacial charge transfer processes. Both these quantum dots are energetically capable of sensitizing TiO_2 films and generating photocurrents in quantum dot solar cells. These two semiconductor nanocrystals exhibit markedly different external quantum efficiencies (~70% for CdSe and ~0.1% for CdTe at 555 nm). Although CdTe with a more favorable conduction band energy (E_{CB} = −1.0 V *vs* NHE) is capable of injecting electrons into TiO_2 faster than CdSe (E_{CB} = −0.6 V *vs* NHE), hole scavenging by a sulfide redox couple remains a major bottleneck. The sulfide ions dissolved in aqueous solutions are capable of scavenging photogenerated holes in photoirradiated CdSe system but not in CdTe. The anodic corrosion and exchange of Te with S dominate the charge transfer at the CdTe interface. Factors that dictate the efficiency and photostability of CdSe and CdTe quantum dots are discussed.

KEYWORDS: quantum dot solar cell · light energy conversion · semiconductor nanocrystals · CdSe · CdTe · photocorrosion · photocurrent generation

The recent interest in utilizing semiconductor nanocrystals (or quantum dots, QDs) for harvesting light energy has drawn great attention toward metal-chalcogenide-based systems.[1−3] Of particular interest are CdX and PbX (X = S, Se, and Te) QDs, which have relatively small bandgaps and thus are capable of harvesting photons in the visible and infrared region.[4,5] These materials have been employed in three different types of quantum dot solar cells: (i) metal junction solar cells,[6−9] (ii) polymer hybrid solar cells,[10−16] and (iii) quantum dot-sensitized solar cells (QDSCs).[17−26] In the metal junction solar cells, charge separation is achieved at metal−semiconductor interface upon visible laser excitation. The polymer hybrid solar cells utilize blends of conducting polymers (*e.g.*, poly(3-hexylthiophene)) and QDs to facilitate charge separation and charge transport. In the case of the QDSCs, excited electrons of semiconductor nanocrystals are injected into a large bandgap semiconductor such as TiO_2 or ZnO, and holes are scavenged by a redox couple (Scheme 1). Despite a recent burst in research activities, the overall power conversion efficiencies have remained below 5%.[17−19] A better understanding of the limiting factors is, therefore, urgently needed to further improve the efficiency of QDSCs.

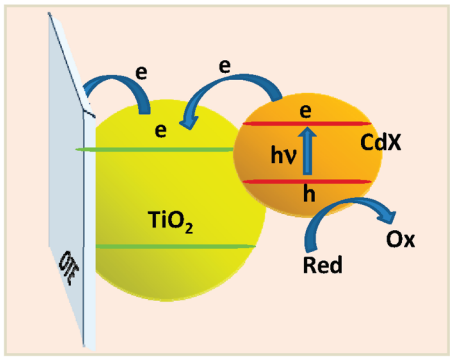

Scheme 1. Charge injection from excited semiconductor nanocrystal, CdX (X = Se or Te) into TiO_2 nanoparticle and scavenging of holes by a red-ox couple in the operation of quantum dot sensitized solar cell.

In recent years, several research groups[18−31] as well as ours[17,32−35] have focused on utilizing the CdSe−TiO_2 system in QDSCs. External quantum efficiencies up to ~80% and power conversion efficiencies up to ~4.2% have been achieved using CdSe nanocrystals as a sensitizer. CdSe QDs linked to TiO_2 in the QDSCs are capable of injecting electrons into TiO_2 nanoparticles with rate constants as high as 10^{10} s^{-1}.[36] By controlling the size of these semiconductor QDs, one can readily tune the band energies as well as the photoresponse of the solar cell.[17,37] CdSe nanocrystals anchored onto TiO_2 nanoparticles generate stable photocurrents during the operation of solar cells as sulfide ions present in the electrolyte regenerate the sensitizer by scavenging holes of the valence band.

Another important aspect of QDSCs is the role of a sulfide/polysulfide (S^{2-}/S_n^{2-}) couple in stabilizing the

*Address correspondence to pkamat@nd.edu.

Received for review March 31, 2009 and accepted April 27, 2009.

Published online May 12, 2009.
10.1021/nn900324q CCC: $40.75

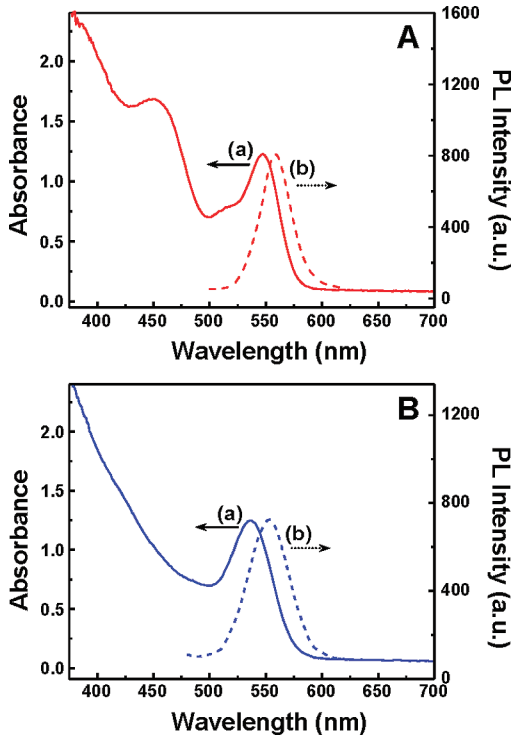

Figure 1. Absorption and emission spectra of (A) CdSe and (B) CdTe nanocrystal suspension in toluene. The excitation wavelength was 450 nm.

photoelectrochemical activity of metal chalcogenide electrodes. In early studies with single crystals, several research groups[38−43] established the redox behavior of S^{2-}/S_n^{2-} and other redox couples as well as their participation in interfacial charge transfer process. An interesting fact is that in the presence of the S^{2-}/S_n^{2-} redox couple, a significant shift in the conduction band energies toward negative potentials takes place. This effect originates from the surface interaction with sulfide (electron donor) as the metal chalcogenide surface becomes negatively charged.[38,43,44] For example, the conduction band energies of CdS, CdSe, and CdTe in neutral solutions are −0.8, −0.6, and −1.0 V *vs* normal hydrogen electrode (NHE), respectively.[45] When in contact with sulfide, however, these conduction bands shift to −1.0, −1.2, and −1.25 V (*vs* NHE), respectively.[38] In all these cases, anodic corrosion is thermodynamically

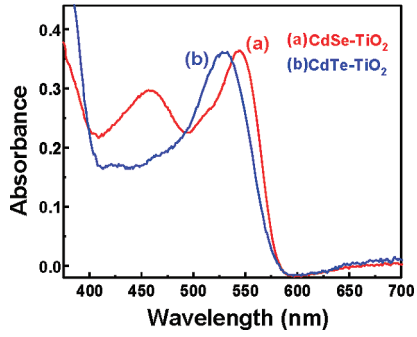

Figure 2. Diffuse reflectance absorption spectra of CdSe−TiO_2 and CdTe−TiO_2 films deposited on OTE (optically transparent electrode).

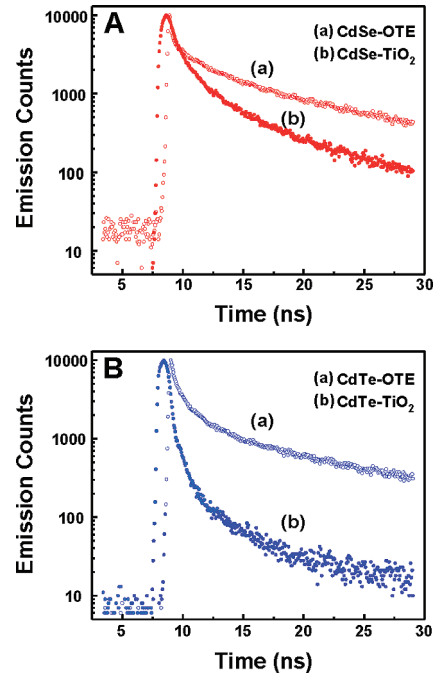

Figure 3. Fluorescence emission decay of (A) CdSe and (B) CdTe QDs: (a) deposited on glass (OTE) and (b) linked onto TiO_2 film cast on OTE slide. The measurements were carried out in the absence of electrolyte.

feasible as the photogenerated holes can participate in surface oxidation. The presence of sulfide, however, brings in stability because it scavenges the holes with a competitive kinetics. If the scavenging of holes by the redox couple is kinetically slow, the anodic corrosion is expected to dominate the hole oxidation process.

CdTe is a widely used semiconductor in thin film solar cell modules with exceptional photostability. First Solar Inc. (Perrysburg, Ohio), which manufactures low cost CdTe-based thin film solar modules, offers a 25 year performance warranty. CdTe has a bulk bandgap of 1.54 eV with conduction and valence band energies at −1.0 and 0.54 V (*vs* NHE), respectively. These characteristics render CdTe an ideal material for harvesting near-infrared and visible photons in QDSCs. Despite a successful employment of CdTe nanocrystals on CdTe/CdSe heterojuction solar cell,[46] the utilization of CdTe QDs for solar energy conversion has been limited especially in photoelectrochemical cells (*i.e.*, cells with liquid electrolytes).[47−54] To exploit CdTe QDs in the QDSC, we have undertaken a systematic study to probe their photophysical and photoelectrochemical behavior by linking them to TiO_2 nanoparticles. The results that compare the performance of CdTe−TiO_2 with CdSe−TiO_2 system are presented in this study.

RESULTS AND DISCUSSION

Optical Properties of QD Solution and QD Films. CdSe and CdTe nanoparticles exhibit size quantization properties, and their absorption can be tuned by controlling their size. Figure 1 panels A and B show the absorption and photoluminescence properties of CdSe and CdTe

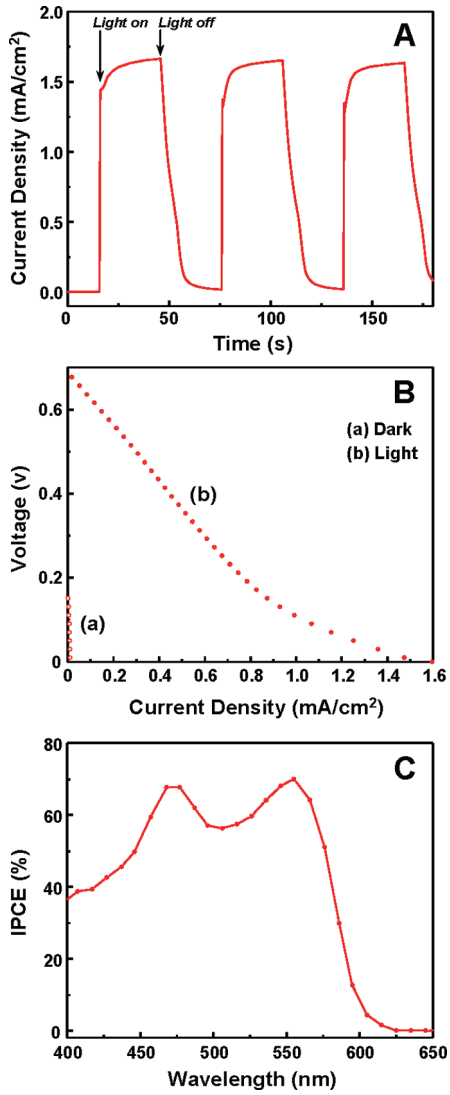

Figure 4. Photoelectrochemical behavior of CdSe−TiO_2 electrode: (A) photocurrent response to ON−OFF cycles of visible illumination (λ > 420 nm, 50 mW/cm²), (B) current−voltage characteristics obtained with varying load: (a) dark and (b) illuminated, and (C) photocurrent action spectra. Electrolyte: 0.1 M Na_2S. (Total illuminated area was 0.3 cm²).

QDs dispersed in toluene, respectively. CdSe QDs exhibit typical absorption characteristics (*i.e.*, a sharp first excitonic peak ($1S_{3/2}1S_e$) at 547 nm with a broad second excitonic peak ($1P_{3/2}1P_e$) at 450 nm) and a band-edge emission with a maximum at 558 nm. The maximum absorption and emission of CdTe QDs appear at similar positions (534 and 553 nm, respectively). From the sizing curve we estimate the particle diameter of CdSe and CdTe to be 3.0 and 3.2 nm, respectively.[55,56] The size selection for these two nanocrystals was made such that we could obtain closely matching absorption and emission bands in the visible region.

Figure 2 shows the absorption spectra of CdSe and CdTe nanoparticles linked to nanostructured TiO_2 films cast on an optically transparent electrode (OTE). The absorption features of these films with maxima at 545 and 531 nm are similar to those observed in toluene solution. This further assures that the linked CdSe and CdTe nanocrystals retain their absorption characteristics following their deposition onto TiO_2 film.

TABLE 1. Emission Decay Analysis of CdSe and CdTe QDs Deposited on OTE and TiO_2, Respectively[a]

	a_1	τ_1(ns)	a_2	τ_2(ns)	a_3	τ_3(ns)	$\langle\tau\rangle$ (ns)	χ^2
CdSe−OTE	0.12	0.15	0.16	1.74	0.72	8.57	6.50 ± 0.14	1.32
CdSe−TiO_2	0.20	0.18	0.38	1.04	0.42	5.02	2.50 ± 0.03	1.39
CdTe−OTE	0.11	0.27	0.26	1.34	0.63	8.54	5.80 ± 0.16	1.34
CdTe−TiO_2	0.81	0.10	0.11	0.63	0.08	3.72	0.45 ± 0.06	1.58

[a]The decay traces in Figure 3 were analyzed using the equation: $F(t) = a_1e^{-k\tau 1} + a_2e^{-k\tau 2} + a_3e^{-k\tau 3}$.

Charge Injection into TiO_2 Nanoparticles. When excited with visible light, the CdSe and CdTe nanocrystals exhibit bright emission as the photogenerated charge carriers recombine. Significant quenching of the emission could be seen upon linking these nanocrystals to TiO_2 nanoparticles. As shown in our earlier studies,[17,33,36] such quenching of the emission represents the electron injection from excited CdSe into TiO_2 nanoparticles. The rate of charge recombination and charge injection processes (reactions 1 and 2, respectively) dictate the emission decay of CdSe and CdTe nanoparticles.

$$CdX\,(X = Se\ or\ Te) + h\nu \rightarrow CdX(e + h) \rightarrow CdX + h\nu' \quad (1)$$

$$CdX(e + h) + TiO_2 \rightarrow CdX(h) + TiO_2(e) \quad (2)$$

Figure 3 shows the emission decay of CdSe and CdTe nanoparticles anchored to TiO_2 films and plain OTEs, recorded with 373 nm diode laser excitation. The samples were stable enough to record luminescence measurements under low intensity excitations. (No self-degradation was observed during these measurements.) As observed in the previous studies, both heterogeneity of samples and varying degree of surface defects introduce multiexponential decay behavior to the charge recombination process.[17,33,36] The luminescence decay was multiexponential, and the traces were fitted with three exponential kinetics. The analysis of the lifetime measurements of CdSe and CdTe QDs on glass and TiO_2 surface are summarized in Table 1. For comparison purpose, we also determined the average emission lifetimes based on eq 3.[57]

$$\langle\tau\rangle = \sum(a_i\tau_i^2)/\sum(a_i\tau_i) \quad (3)$$

On the conducting glass surface (OTE), we observed relatively long-lived emission with the average lifetimes

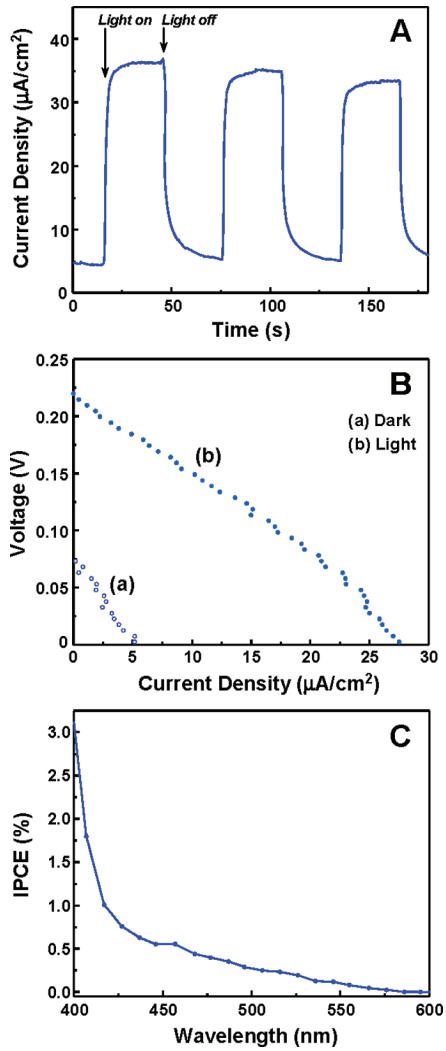

Figure 5. Photoelectrochemical behavior of CdTe−TiO_2 electrode. (A) Photocurrent response to ON−OFF cycles of visible illumination (λ > 420 nm, 50 mW/cm²). (B) Current−voltage characteristics obtained with varying load: (a) dark and (b) illuminated. (C) Photocurrent action spectra. Electrolyte, 0.1 M Na_2S (total illuminated area was 0.3 cm²).

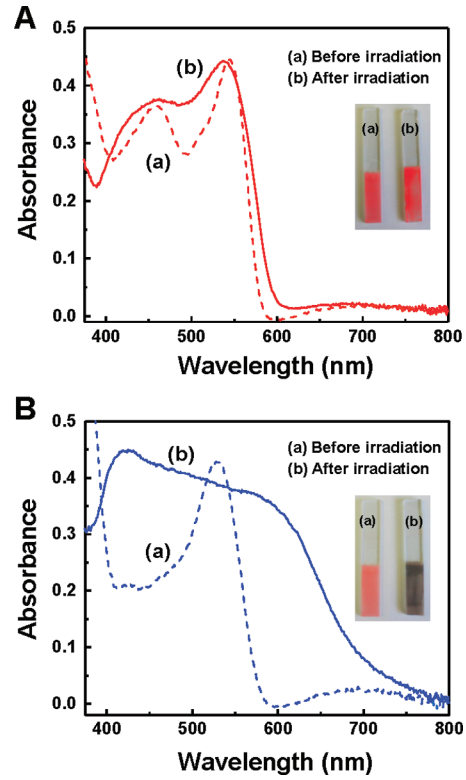

Figure 6. Diffuse reflectance UV−vis absorption spectra of (A) CdSe−TiO_2 and (B) CdTe−TiO_2 films (a) before and (b) after irradiation with visible light and during the operation of photoelectrochemical cell containing 0.1 M Na_2S. Inset: photographs of (top) CdSe−TiO_2 and (bottom) CdTe−TiO_2 films (a) before and (b) after photoelectrochemical measurements.

of 6.5 and 5.8 ns for CdSe and CdTe, respectively. Significant decreases in lifetime, however, were observed on the TiO_2 surface with average lifetimes of 2.5 and 0.45 ns for CdSe and CdTe systems, respectively. The interaction between CdTe QDs and TiO_2 is greater than that of CdSe QDs and TiO_2, as evident from the decreased lifetime in these experiments. In particular, the fast component, which contributes nearly 80% of the decay, shows a major decrease in lifetime from 0.27 to 0.10 ns in the CdTe−TiO_2 system.

We determined the apparent rate constants for the charge injection process, k_{et}, by comparing the lifetimes of CdX (X = Se or Te) on glass ($\langle\tau_0\rangle$) and TiO_2 surface ($\langle\tau\rangle$) using eq 4.

$$k_{et} = 1/\langle\tau\rangle - 1/\langle\tau_0\rangle \quad (4)$$

The apparent rate constants for charge injection into TiO_2 particles (reaction 2) are 2.4×10^8 s^{-1} for CdSe and 2.1×10^9 s^{-1} for CdTe, respectively. It is evident that the charge injection from the excited CdTe into TiO_2 occurs with a rate constant that is an order of magnitude greater than that between CdSe and TiO_2. As will be discussed in a later section, the difference in conduction band positions between CdTe and CdSe contributes to such a difference in the rate constant. It should be noted that the above estimation of average lifetimes takes into account both short- and long-lived components. A major fraction of the charge injection process occurs with a greater rate constant (as high as 10^{10} s^{-1}) if we compare only the fast component of the emission decay. For example, ~80% of the emission decay of CdTe QDs on TiO_2 surface occurs with a lifetime of 0.10 ns, indicating the major fraction of the charge injection event occurs on an ultrafast time scale.

Photoelectrochemical Measurements. The effectiveness of charge injection from excited CdX (X = Se or Te) nanoparticles into TiO_2 films was further evaluated by employing them in a photoelectrochemical cell. The use of CdSe QDs as a sensitizer in photoelectrochemical cells has been previously investigated by several research groups.[17−28,32−35] Our earlier studies[5,17] demonstrated

the ability to tune the photoresponse of the photoelectrochemical cell by controlling the size of QDs.

Figure 4 shows a typical analysis of the electrode performance of the CdSe−TiO_2 electrode. A thick film of TiO_2 particles (~10 μm) cast on an OTE allowed us to link a relatively large concentration of CdSe QDs through 3-mercaptopropionic acid linker. The role of the linker in obtaining monodispersed particle adsorption and achieving a higher IPCE was recently discussed.[29] Upon illumination with visible light filtered through a 420 nm cutoff filter, we obtained a photocurrent of 1.6 mA/cm^2 and a photovoltage of 0.7 V. The appearance of the photocurrents was prompt, and the photocurrent generation was steady during ON−OFF cycles of the illumination.

The *I*−*V* characteristics show a steep decrease at higher loads, thus indicating possible mass transfer limitation of S^{2-} in the nanopores. The incident photocurrent to charge carrier generation efficiency (IPCE %) was evaluated by monitoring short circuit currents at different incident wavelengths and using

$$\text{IPCE}(\%) = 1240(I_{sc}/I_{inc})100 \quad (5)$$

where I_{sc} and I_{inc} refer to a short circuit current and energy of incident monochromatic light, respectively. The photoresponse of the electrode below 600 nm confirms that the origin of the photocurrent generation is CdSe excitation. The two peaks seen around 550 and 450 nm closely match the absorption peaks seen with the two excitonic transitions in the absorption spectrum. The drop in the photocurrent response is likely to arise from nonuniform absorption of the light because of the high absorbance values (>1).

Another interesting point is our ability to achieve high IPCE values for the CdSe-sensitized quantum dot solar cells. Nearly 70% of IPCE values seen in the present experiment are the highest among the linked CdSe solar cells (*i.e.*, linked to TiO_2 *via* linker molecules such as 3-mercaptopropionic acid).[17,18,26,29,33] Relatively high loading of CdSe QDs with the absorbance of ~1 at the excitonic transition wavelength of 550 nm, achieved by the optimized linking procedure, has allowed us to capture more photons and generate a greater numbers of charge carriers.

A different scenario emerged when we employed CdTe QDs as a sensitizer. The method employed to anchor these QDs to TiO_2 nanostructured films *via* 3-mercaptopropionic acid linker was similar to that employed in the CdSe-modified TiO_2 electrodes. We were also able to achieve relatively high absorbance (>1) at the excitonic band. When the CdTe−TiO_2 electrode was employed in the photoelectrochemical cell, however, a significantly lower performance with a maximum photocurrent of only ~28 μA/cm^2 and an open circuit voltage of ~0.22 V was observed (Figure 5). The *I*−*V* characteristics also reflected a similar trend of the poor performance.

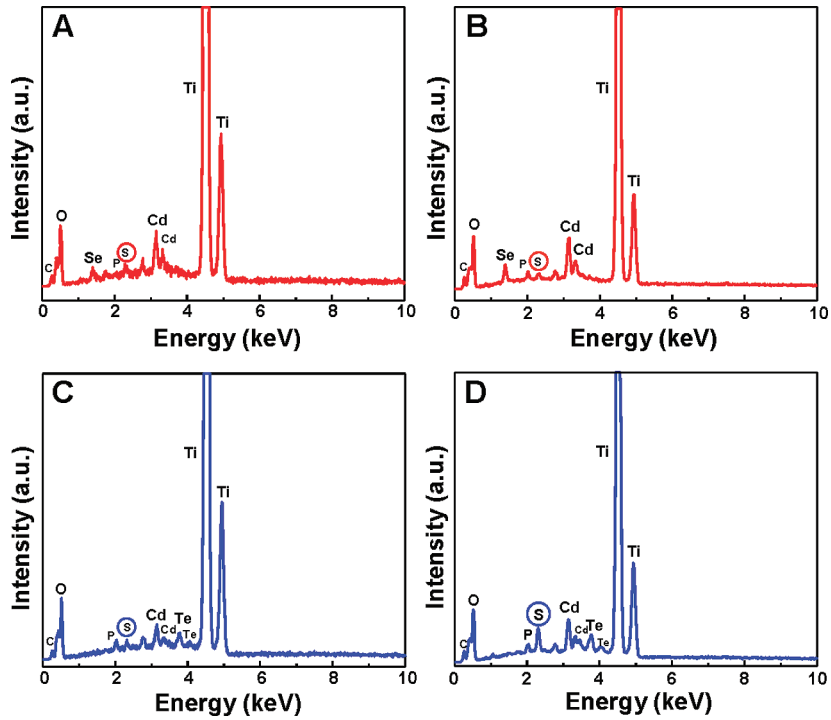

Figure 7. SEM-EDS analysis of (A and B) CdSe−TiO_2 and (C and D) CdTe−TiO_2 electrodes. The analysis was conducted before (A and C) and after (B and D) using the electrode in a photoelectrochemical cell containing 0.1 M Na_2S and irradiating the cell with visible light for 15 min.

The photocurrents at different incident wavelengths were recorded to evaluate the photoresponse of the CdTe−TiO_2 electrode. We see that the photocurrent response below 600 nm is in good agreement with the onset absorption of CdTe QDs. The photocurrent response at the excitonic transitions, however, is less resolved and merely appears as shoulders. The maximum IPCE observed above 425 nm is less than 1%. These results indicate that the performance of the QDSC based on CdTe nanocrystals and the S^{2-}/S_n^{2-} redox couple does not exhibit any viability for developing competitive devices. To assess the factors that are detrimental to the performance of CdTe nanocrystals, we further evaluated the photostability aspects of the CdTe−TiO_2 electrode.

Photostability of CdSe and CdTe Nanocrystals in QDSCs. Figure 6 shows the absorption spectra of CdSe−TiO_2 and CdTe−TiO_2 electrodes before and after their operation in the photoelectrochemical cell containing 0.1 M Na_2S. The electrodes were exposed to visible light (λ > 420 nm) for 15 min under short circuit con-

ditions. The insets show the photograph of each electrode before and after irradiation. It is evident from these pictures that significant changes in the coloration are seen in the CdTe−TiO_2 electrode. The absorption spectra reflect the changes in the spectral characteristics. In the case of the CdSe−TiO_2 electrode, the spectral changes are minimal; both excitonic transitions are retained with a slight broadening of the peaks. The CdTe−TiO_2 electrode, on the other hand, shows a marked change with absorption extending to 800 nm. The spectral features indicate that the CdTe nanocrystals have undergone transformations during the photoirradiation when in contact with Na_2S solution; we also observed that even prior to photoirradiation, CdTe QDs start to react with Na_2S, and the transformation was accelerated under photoirradiation. Although CdTe itself shows remarkable photostability as evident from its use in thin film solar cells, the photodegradation is likely to arise from its reactivity in the aqueous sulfide solution.

Role of Sulfide in Scavenging Photogenerated Holes. The sulfide/polysulfide (S^{2-}/S_n^{2-}) redox couple has been extensively studied for its ability to interact with metal chalcogenides.[38,41,58−60] During the early photoelectrochemical investigation of single crystal metal chalcogenide electrodes, it was pointed out that the redox couple, S^{2-}/S_n^{2-}, can stabilize CdS and CdSe, but not CdTe.[38,61] During the photoirradiation of CdX (X = Se or Te) in the presence of the sulfide electrolyte, it is possible to expect one of four interfacial reactions (reactions 6−9) to dominate after the initial charge separation (reaction 2).

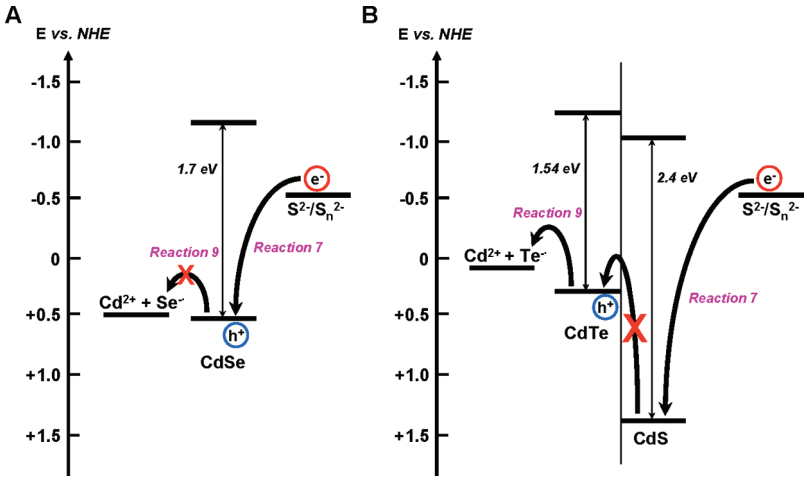

Scheme 2. Energy diagram of (A) CdSe and (B) CdTe/CdS in Na_2S solution. Note that band gaps and positions of CdSe and CdTe/CdS are depicted on the basis of their bulk values. Although quantum dots used in this study have larger bandgap, the relative positions of valence band are likely to be close to the bulk bandgap. Most of the increase is reflected in the shift of conduction band. In addition, the redox potential of Na_2S may be negatively shifted by ~0.1 V, assuming a trace of sulfur formed during the cell operation.

anodic decomposition: $CdX(e + h) \rightarrow Cd^0 + X^0$ (6)

scavenging of holes: $CdX(h) + S^{2-} \rightarrow CdX + S \xrightarrow{S^{2-}} CdX + S_n^{2-}$ (7)

substitution reaction: $CdX(h) + S^{2-} \rightarrow CdS + X^{2-}$ (8)

anodic corrosion: $CdX(h) \rightarrow Cd^{2+} + X^{-\bullet}$ (9)

The EDS analysis of the CdSe−TiO_2 and CdTe−TiO_2 electrodes was conducted with a scanning electron microscope. The results obtained with the electrodes before and after the visible light irradiation (corresponding to the experimental conditions in Figure 6) are shown in Figure 7.

The CdSe−TiO_2 electrodes before and after irradiation show the peaks corresponding to Cd and Se arising from CdSe nanocrystals. These peaks are accompanied by Ti and O from the TiO_2 that are linked to CdSe. The small peak seen for S arises from the linker molecule, 3-mercaptopropionic acid. The relative intensity of this peak remains unchanged even after the photoirradiation. No new features in the photoirradiated sample could be seen in the CdSe−TiO_2 films, thus confirming its photostability to the photoirradiation in the presence of Na_2S solution. In the case of CdTe−TiO_2 electrodes, characteristic peaks corresponding to Cd, Te, S, Ti, and O elements were observed. The major difference, however, resides in the increase in the relative intensity of S peak after the photoirradiation. This observation suggests incorporation of S into the CdTe nanocrystal as it interacts with S^{2-} present in the electrolyte. The substitution reaction 8 thus leads to the formation of CdS layers on the surface of CdTe nanocrystals. The differences seen between the CdSe and CdTe electrodes in the photoirradiated samples highlight the reactivity of photogenerated holes in these two semiconductors toward S^{2-}.

Scheme 2 shows the energy levels of CdSe and CdTe with respect to the S^{2-}/S_n^{2-} redox couple. When in contact with the sulfide electrolyte, the conduction band energies of CdSe and CdTe exhibit a shift toward negative potentials. On the basis of the photopotential measurements and Mott−Schotky plots, Ellis et al.[38] measured the conduction band potentials of CdSe and CdTe to be at −1.2 and −1.25 V (*vs* NHE), respectively. The S^{2-}/S_n^{2-} couple having a reduction potential of −0.5 V (*vs* NHE) is, therefore, capable of interacting with the photogenerated holes from both CdSe and CdTe electrodes. The

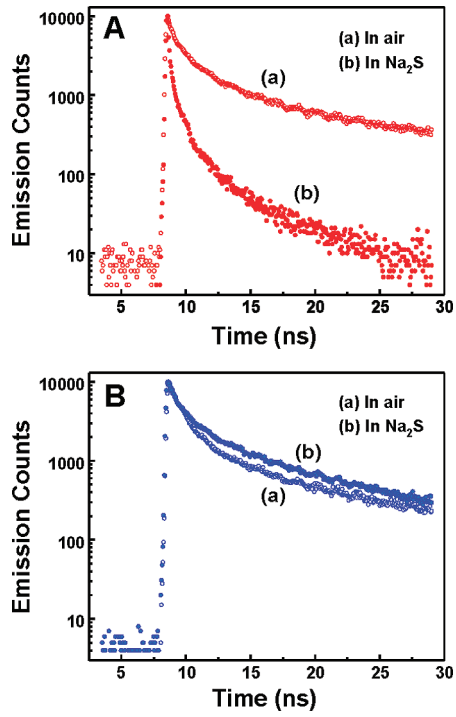

Figure 8. Emission decay of CdSe and CdTe nanocrystals linked to SiO_2 films: (A) CdSe−SiO_2 and (B) CdTe−SiO_2 electrodes (a) in the absence and (b) in contact with 0.1 M Na_2S solution.

other competing reaction is the anodic corrosion (reaction 9) that occurs at potentials of 0.53 V (*vs* NHE) in CdSe and 0.10 V (*vs* NHE) in CdTe, respectively. As illustrated in Scheme 2, the anodic corrosion (reaction 9) is more energetically favored in CdTe than in the CdSe system, thus making CdTe more susceptible to direct oxidation and substitution reaction (reaction 8).

As shown in earlier studies,[38−41] the reactivity of the photogenerated holes with sulfide remains a rate determining factor. The charge transfer with sulfide at the CdSe interface dominates over the anodic corrosion and substitution reactions. In the case of CdTe, the substitution reaction dominates, and the formation of a CdS shell creates a barrier to the hole scavenging from CdTe nanocrystals (Scheme 2). The inability of hole scavenging from CdTe by sulfide thus causes self-destruction.

If indeed the reactivity of sulfide toward the two semiconductors should be different, we should be able to follow it by monitoring the emission decay of CdSe and CdTe. Figure 8 shows the emission decay of CdSe−SiO_2 and CdTe−SiO_2 electrodes in the absence and presence of Na_2S. These traces were analyzed with three exponential decay kinetics, and the results are summarized in Table 2. It is evident that the presence of the sulfide redox couple has a significant effect on the decay of CdSe; the decreased lifetimes indicate the ability of sulfide to scavenge the photogenerated holes. Using eq 4 with the average lifetimes, we obtained an apparent rate constant of 7.7×10^8 s^{-1} for the regeneration of CdSe by the sulfide redox couple (reaction 7). No such quenching of emission, however, was seen in the CdTe system. A small increase in the lifetime is likely due to the formation of CdS shell. These results further support our argument that the formation of CdS shell and inability of S^{2-} to scavenge the photogenerated holes result in the photodegradation of CdTe nanocrystals.

TABLE 2. Emission Decay Analysis[a] of CdSe and CdTe QDs Deposited on SiO_2 in the Absence and Presence of Na_2S Solution, Respectively

	a_1	τ_1 (ns)	a_2	τ_2 (ns)	a_3	τ_3 (ns)	$\langle\tau\rangle$ (ns)	χ^2
CdSe−SiO_2 in air	0.06	0.21	0.32	1.32	0.62	6.46	4.44 ± 0.01	1.70
CdSe−SiO_2 in Na_2S	0.48	0.10	0.33	0.72	0.19	3.78	1.00 ± 0.05	1.20
CdTe−SiO_2 in air	0.02	0.19	0.43	1.06	0.55	6.25	3.88 ± 0.01	1.88
CdTe−SiO_2 in Na_2S	0.06	0.41	0.28	1.47	0.66	7.41	5.35 ± 0.04	1.75

[a]Analyzed with three exponential decay as employed in Table 1.

The results presented here highlight the similarities and contrast the differences between two similar semiconductor systems. Both CdSe and CdTe exhibit size quantization effects, bind strongly to TiO_2 through a linker molecule, and inject electrons into TiO_2 with an ultrafast rate under bandgap excitation. The reactivity of photogenerated holes with the sulfide electrolyte, however, determines their suitability in QDSCs. CdSe remains regenerative during the operation of QDSC as the photogenerated holes are scavenged by S^{2-} ions. A maximum IPCE of 70% shows the suitability of this system in a photoelectrochemical solar cell. The scenario is, however, different for CdTe-based QDSC. The formation of a CdS shell and the inability to scavenge photogenerated holes make CdTe a poor candidate for QDSCs.

We also attempted to use a series of other redox couples in the photoelectrochemical cells as a replacement of the S^{2-}/S_n^{2-} couple (I^{3-}/I^-, ferrocene/ferrocene$^+$, $K_4Fe(CN)_6/K_3Fe(CN)_6$ with/without KCN, Te^{2-}/Te_2^{2-}, and Co complexes ($[Co^{II}(Open)_3](TFSI)_2/[Co^{III}(Open)_3](TFSI)_3$ where Open = 1,10-phenanthroline and TFSI = bis-trifluoromethane sulfoimide). None of these redox couples seems to provide the required photostability for the CdTe QD electrodes; in fact, most of them immediately corrode CdTe QDs even under ambient conditions.

The results shown here present several major challenges to the utilization of CdTe QDs in photoelectrochemical cells. Despite the failure of the use of CdTe QDs in photoelectrochemical cells, we believe that the effort to find suitable hole scavengers must be continued, and the use of CdTe QDs in QDSCs may need to be directed to solid-state solar cells. As previously demonstrated in Alivisatos's work,[46] the exploitation of CdTe nanocrystals for the absorption in far-red and near-IR region is still promising in solid-state solar cells where

the stability issue observed in this work seems to be no critical problem during the cell operation.

CONCLUSIONS

The size-quantized semiconductor particles are attractive for developing next generation solar cells. While the band energies can be tuned through the control of particle size, the conduction and valence bands levels play an important role in dictating capture of photogenerated electrons and holes at the interface. CdTe has a more negative conduction band compared to CdSe and hence injects electrons into TiO_2 nanoparticles at a faster rate. Despite the fast electron injection rate we observed a poor external quantum efficiency (<3%). CdSe, on the other hand, shows a superior performance with nearly 70% quantum efficiency. The difference in the performance of these two systems has been understood based on the position of their valence bands. The energy levels of valence bands are such that redox couples such as a sulfide/polysulfide couple scavenge holes only from CdSe and *not* from CdTe. This failure to scavenge photogenerated holes results in the degradation of CdTe. Hence, the choice of CdTe for the operation of QDSCs (*i.e.*, photoelectrochemical cells) currently poses a serious challenge. Experiments are underway to utilize these semiconductor nanocrystals in metal junction quantum dot solar cells.

EXPERIMENTAL SECTION

Materials. Cadmium oxide (CdO, Aldrich), tetradecylphosphonic acid (TDPA, PCI Synthesis), trioctylphosphine oxide (TOPO, Aldrich), dodecylamine (DDA, Aldrich), octadecene (ODE, Aldrich), selenium (Se, Aldrich), tellurium (Te, Aldrich), and trioctylphosphine (TOP, Aldrich) were used as received to prepare CdSe and CdTe QDs. 3-Mercaptopropionic acid (3-MPA, Aldrich), propionic acid (PA), (3-mercaptopropyl)-trimethoxysilane (3-MPS, Aldrich), titanium (IV) tetraisopropoxide (TTIP, Aldrich), titanium (IV) tetrachloride ($TiCl_4$, Strem), P-25 TiO_2 powder (Degussa), and colloidal SiO_2 suspension (Nalco2327) were used to prepare QD films. Conducting glass slides (Pilkington) were used as an optically transparent electrode (OTE).

Synthesis of CdSe and CdTe QDs. CdSe and CdTe QDs were prepared by the commonly employed hot injection method with some modifications.[62] In CdSe QD synthesis, CdO (0.39 mmol), TOPO (5.2 mmol), TDPA (1.1 mmol), and DDA (5.4 mmol) were degassed at 110 °C for 1 h and then heated under nitrogen to 315 °C to completely dissolve the precursors. TOPSe (0.25 mmol Se dissolved in 4.25 mL of TOP) was subsequently injected into the hot solution to initiate the reaction. After 2 min of growth at 270 °C, the QD solution was cooled to room temperature, washed three times with a mixture of methanol and toluene, and dissolved in toluene for use. CdTe QDs were, on the other hand, prepared in a noncoordinating solvent (ODE).[56] A mixture of TOPTe (0.05 mmol Te dissolved in 0.7 mL of TOP) and ODE (2.45 mL) was injected into a clear cadmium complex solution containing CdO (0.1 mmol), TDPA (0.2 mmol), and ODE (5 mL) at 300 °C, and solution was maintained at 275 °C for 3 min for particle growth. The CdTe QDs were purified with a mixture of isopropyl alcohol and toluene, and they were finally stored in toluene.

Preparation of CdSe and CdTe QD Films. QD-TiO_2 films were prepared as follows: TiO_2 paste was prepared by sonicating P-25 TiO_2 powder suspended in 0.1 M TTIP solution in ethanol in an ice bath for 1 h. The paste was then applied to an OTE by the doctor blade technique. The dried film was dipped into 0.05 M $TiCl_4$ solution at 70 °C for 30 min, dried in air, and annealed under air at 450 °C for 30 min. The annealed TiO_2 film was dipped into a N_2-purged acetonitrile solution containing 0.14 M 3-mercaptopropionic acid and 0.86 M propionic acid for 24 h, subsequently washed with acetonitrile and toluene, and placed into a N_2-purged QD solution for 48 h. The use of a mixture of 3-mercaptopropionic acid and propionic acid tends to minimize interlayer disulfide formation and increase QD adsorption, as noted previously.[63] To prepare thin QD film on an OTE, QD solutions were directly drop-casted onto a warm OTE and dried. QD-SiO_2 films were prepared in a similar fashion as in the preparation of QD-TiO_2 films. Colloidal SiO_2 suspension was diluted with water and sprayed onto a hot OTE. The SiO_2 film was annealed under air at 400 °C for 2 h and subsequently placed into a N_2-purged toluene solution containing 0.2 M (3-mercaptopropyl)-trimethoxysilane for 1 h. After being washed with toluene, the film was dipped into a N_2-purged QD solution for 48 h. All films were stored under N_2 in the dark before using them in various experimental evaluations. The resulting films will hereafter be referred to as CdSe−TiO_2 (or CdTe−TiO_2), CdSe−OTE (or CdTe−OTE), and CdSe−SiO_2 (or CdTe−SiO_2).

Characterization. UV−vis absorption and fluorescence emission spectra of CdSe and CdTe QD solutions were recorded using a Varian CARY50 Bio UV−visible spectrophotometer and a SLM-S 8000 spectrofluorometer, respectively. Fluorescence emission lifetime measurements were carried out using a Horiba Jobin Yvon single photon counting system with a diode laser (373 nm, 250 kHz repetition, 1.1 ns pulse width) as an excitation source. Diffuse reflectance UV−vis spectra of CdSe−TiO_2 and CdTe−TiO_2 films were obtained using a Shimadzu UV-3101 PC spectrophotometer. Energy dispersive X-ray spectroscopy (EDS) was carried out with a Hitachi S-4500 scanning electron microscopy.

Photoelectrochemical Measurements. Photoelectrochemical behavior of QD-TiO_2 films was investigated using a two-armed cell with a Pt-gauze counter-electrode in a N_2-purged, aqueous 0.1 M Na_2S solution as a redox couple (note: polarization of Pt-gause counter-electrode was not measured in this experiment). Photocurrent measurements and $I-V$ characteristics were carried out using a Keithley 617 programmable electrometer along with collimated, filtered light ($\lambda > 420$ nm, 50 mW/cm^2) from an Oriel 450 W xenon arc lamp. For incident photon to charge carrier generation efficiency (IPCE) measurement, a Bausch and Lomb high-intensity grating monochromator was introduced into the light path to select an excitation wavelength.

Acknowledgment. The research described herein was supported by the Office of Basic Sciences of the U.S. Department of Energy. This is contribution number NDRL 4800 from the Notre Dame Radiation Laboratory.

REFERENCES AND NOTES

1. Kamat, P. V. Quantum Dot Solar Cells. Semiconductor Nanocrystals as Light Harvesters. *J. Phys. Chem. C* **2008**, *112*, 18737–18753.
2. Hodes, G. Comparison of Dye- and Semiconductor-Sensitized Porous Nanocrystalline Liquid Junction Solar Cells. *J. Phys. Chem. C* **2008**, *112*, 17778–17787.
3. Harris, C. T.; Kamat, P. V. Photocatalysis with CdSe Nanoparticles in Confined Media: Mapping Charge Transfer Events in the Subpicosecond to Second Timescales. *ACS Nano* **2009**, *3*, 682–690.
4. Scholes, G. D. Insights into Excitons Confined to Nanoscale Systems: Electron-Hole Interaction, Binding Energy, and Photodissociation. *ACS Nano* **2008**, *2*, 523–537.
5. Baker, D. R.; Kamat, P. V. Photosensitization of TiO_2 Nanostructures with CDs Quantum Dots. Particulate *versus* Tubular Support Architectures. *Adv. Funct. Mater.* **2009**, *19*, 805–811.

6. Luther, J. M.; Law, M.; Beard, M. C.; Song, Q.; Reese, M. O.; Ellingson, R. J.; Nozik, A. J. Schottky Solar Cells Based on Colloidal Nanocrystal Films. *Nano Lett.* **2008**, *8*, 3488–3492.
7. Law, M.; Beard, M. C.; Choi, S.; Luther, J. M.; Hanna, M. C.; Nozik, A. J. Determining the Internal Quantum Efficiency of PbSe Nanocrystal Solar Cells with the Aid of an Optical Model. *Nano Lett.* **2008**, *8*, 3904–3910.
8. Koleilat, G. I.; Levina, L.; Shukla, H.; Myrskog, S. H.; Hinds, S.; Pattantyus-Abraham, A. G.; Sargent, E. H. Efficient, Stable Infrared Photovoltaics Based on Solution-Cast Colloidal Quantum Dots. *ACS Nano* **2008**, *2*, 833–840.
9. Istrate, E.; Hoogland, S.; Sukhovatkin, V.; Levina, L.; Myrskog, S.; Smith, P. W. E.; Sargent, E. H. Carrier Relaxation Dynamics in Lead Sulfide Colloidal Quantum Dots. *J. Phys. Chem. B* **2008**, *112*, 2757–2760.
10. Ginger, D. S.; Greenham, N. C. Photoinduced Electron Transfer from Conjugated Polymers to CdSe Nanocrystals. *Phys. Rev. B* **1999**, *59*, 10622–10629.
11. Zhang, J.; Coombs, N.; Kumacheva, E.; Lin, Y.; Sargent, E. H. A New Approach to Hybrid Polymer−Metal and Polymer−Semiconductor Particles. *Adv. Mater.* **2003**, *15*, 1756–1759.
12. Bartholomew, G. P.; Heeger, A. J. Infiltration of Regioregular Poly[2,2′-(3-Hexylthiopene)] into Random Nanocrystalline TiO_2 Networks. *Adv. Funct. Mater.* **2005**, *15*, 677–682.
13. Gur, I.; Fromer, N. A.; Chen, C. P.; Kanaras, A. G.; Alivisatos, A. P. Hybrid Solar Cells with Prescribed Nanoscale Morphologies Based on Hyperbranched Semiconductor Nanocrystals. *Nano Lett.* **2007**, *7*, 409–414.
14. Wang, L.; Liu, Y.; Jiang, X.; Qin, D.; Cao, Y. Enhancement of Photovoltaic Characteristics Using a Suitable Solvent in Hybrid Polymer/Multiarmed CdS Nanorods Solar Cells. *J. Phys. Chem. C* **2007**, *111*, 9538–9542.
15. Wang, M. F.; Kumar, S.; Lee, A.; Felorzabihi, N.; Shen, L.; Zhao, F.; Froimowicz, P.; Scholes, G. D.; Winnik, M. A. Nanoscale Co-organization of Quantum Dots and Conjugated Polymers Using Polymeric Micelles As Templates. *J. Am. Chem. Soc.* **2008**, *130*, 9481–9491.
16. Boucle, J.; Chyla, S.; Shaffer, M. S. P.; Durrant, J. R.; Bradley, D. D. C.; Nelson, J. Hybrid Bulk Heterojunction Solar Cells Based on Blends of TiO_2 Nanorods and P3HT. *C. R. Phys.* **2008**, *9*, 110–118.
17. Kongkanand, A.; Tvrdy, K.; Takechi, K.; Kuno, M. K.; Kamat, P. V. Quantum Dot Solar Cells. Tuning Photoresponse through Size and Shape Control of CdSe−TiO_2 Architecture. *J. Am. Chem. Soc.* **2008**, *130*, 4007–4015.
18. Lee, H. J.; Yum, J.-H.; Leventis, H. C.; Zakeeruddin, S. M.; Haque, S. A.; Chen, P.; Seok, S. I.; Grätzel, M.; Nazeeruddin, M. K. CdSe Quantum Dot-Sensitized Solar Cells Exceeding Efficiency 1% at Full-Sun Intensity. *J. Phys. Chem. C* **2008**, *112*, 11600–11608.
19. Shen, Q.; Kobayashi, J.; Diguna, L. J.; Toyoda, T. Effect of ZnS Coating on the Photovoltaic Properties Of CdSe Quantum Dot-Sensitized Solar Cells. *J. Appl. Phys.* **2008**, *103*, 084304.
20. Si, H. Y.; Sun, Z. H.; Zhang, H. L. Photoelectrochemical Response from CdSe-Sensitized Anodic Oxidation TiO_2 Nanotubes. *Colloids Surf., Part A* **2008**, *313*, 604–607.
21. Tena-Zaera, R.; Katty, A.; Bastide, S.; Levy-Clement, C. Annealing Effects on the Physical Properties of Electrodeposited ZnO/CdSe Core-Shell Nanowire Arrays. *Chem. Mater.* **2007**, *19*, 1626–1632.
22. Chong, S. V.; Suresh, N.; Xia, J.; Al-Salim, N.; Idriss, H. TiO_2 Nanobelts/CdSSe Quantum Dots Nanocomposite. *J. Phys. Chem. C* **2007**, *111*, 10389–10393.
23. Lee, J. C.; Sung, Y. M.; Kim, T. G.; Choi, H. J. TiO_2-CdSe Nanowire Arrays Showing Visible-Range Light Absorption. *Appl. Phys. Lett.* **2007**, *91*, 113104.
24. Mora-Sero, I.; Bisquert, J.; Dittrich, T.; Belaidi, A.; Susha, A. S.; Rogach, A. L. Photosensitization of TiO_2 Layers with CdSe Quantum Dots: Correlation between Light Absorption and Photoinjection. *J. Phys. Chem. C* **2007**, *111*, 14889–14892.
25. Niitsoo, O.; Sarkar, S. K.; Pejoux, C.; Ruhle, S.; Cahen, D.; Hodes, G. Chemical Bath Deposited Cds/CdSe-Sensitized Porous TiO_2 Solar Cells. *J. Photochem. Photobiol. A* **2006**, *181*, 306–313.
26. Leschkies, K. S.; Divakar, R.; Basu, J.; Enache-Pommer, E.; Boercker, J. E.; Carter, C. B.; Kortshagen, U. R.; Norris, D. J.; Aydil, E. S. Photosensitization of ZnO Nanowires with CdSe Quantum Dots for Photovoltaic Devices. *Nano Lett.* **2007**, *7*, 1793–1798.
27. Weiss, E. A.; Porter, V. J.; Chiechi, R. C.; Geyer, S. M.; Bell, D. C.; Bawendi, M. G.; Whitesides, G. M. The Use of Size-Selective Excitation to Study Photocurrent through Junctions Containing Single-Size and Multi-Size Arrays of Colloidal CdSe Quantum Dots. *J. Am. Chem. Soc.* **2008**, *130*, 83–92.
28. Sun, B.; Findikoglu, A. T.; Sykora, M.; Werder, D. J.; Klimov, V. I. Hybrid Photovoltaics Based on Semiconductor Nanocrystals and Amorphous Silicon. *Nano Lett.* **2009**, *9*, 1235–1241.
29. Guijarro, N.; Lana-Villarreal, T.; Mora-Seró, I.; Bisquert, J.; Gómez, R. CdSe Quantum Dot-Sensitized TiO_2 Electrodes: Effect of Quantum Dot Coverage and Mode of Attachment. *J. Phys. Chem. C* **2009**, *113*, 4208–4214.
30. Lee, Y.-L.; Huang, B.-M.; Chien, H.-T. Highly Efficient CdSe-Sensitized TiO_2 Photoelectrode for Quantum-Dot-Sensitized Solar Cell Applications. *Chem. Mater.* **2008**, *20*, 6903–6905.
31. Lee, Y.-L.; Lo, Y.-S. Highly Efficient Quantum-Dot-Sensitized Solar Cell Based on Co-sensitization of CdS/CdSe. *Adv. Funct. Mater.* **2009**, *19*, 604–609.
32. Liu, D.; Kamat, P. V. Electrochemical Rectification in CdSe + TiO_2 Coupled Semiconductor Films. *J. Electroanal. Chem. Interfacial Electrochem.* **1993**, *347*, 451–456.
33. Robel, I.; Subramanian, V.; Kuno, M.; Kamat, P. V. Quantum Dot Solar Cells. Harvesting Light Energy with CdSe Nanocrystals Molecularly Linked to Mesoscopic TiO_2 Films. *J. Am. Chem. Soc.* **2006**, *128*, 2385–2393.
34. Brown, P.; Kamat, P. V. Quantum Dot Solar Cells. Electrophoretic Deposition of CdSe-C_{60} Composite Films and Capture of Photogenerated Electrons with nC_{60} Cluster Shell. *J. Am. Chem. Soc.* **2008**, *130*, 8890–8891.
35. Tvrdy, K.; Kamat, P. Substrate Driven Photochemistry of CdSe Quantum Dot Films: Charge Injection and Irreversible Transformation on Oxide Surfaces. *J. Phys. Chem. C* **2009**, *113*, 3765–3772.
36. Robel, I.; Kuno, M.; Kamat, P. V. Size-Dependent Electron Injection from Excited CdSe Quantum Dots into TiO_2 Nanoparticles. *J. Am. Chem. Soc.* **2007**, *129*, 4136–4137.
37. Weiss, E. A.; Chiechi, R. C.; Geyer, S. M.; Porter, V. J.; Bell, D. C.; Bawendi, M. G.; Whitesides, G. M. Size-Dependent Charge Collection in Junctions Containing Single-Size and Multi-Size Arrays of Colloidal CdSe Quantum Dots. *J. Am. Chem. Soc.* **2008**, *130*, 74–82.
38. Ellis, A. B.; Kaiser, S. W.; Bolts, J. M.; Wrighton, M. S. Study of n-Type Semiconducting Cadmium Chalcogenide-Based Photoelectrochemical Cells Employing Polychalcogenide Electrolytes. *J. Am. Chem. Soc.* **1977**, *99*, 2839–2848.
39. Cahen, D.; Hodes, G.; Manassen, J. S/Se Substitution in Polycrystalline CdSe Photoelectrodes. *J. Electrochem. Soc.* **1978**, *125*, 1623–1628.
40. Tenne, R.; Lando, D.; Mirovsky, Y.; Mueller, N.; Manassen, J.; Cahen, D.; Hodes, G. The Relation between Performance and Stability of Cd−Chalcogenide/Polysulfide Photoelectrochemical Cells. The Effect of Potential. *J. Electroanal. Chem. Interfacial Electrochem.* **1983**, *143*, 103–112.
41. Hodes, G.; Miller, B. Thermodynamic Stability of II−VI Semiconductor−Polysulfide Photoelectrochemical Systems. *J. Electrochem. Soc.* **1986**, *133*, 2177–2180.
42. Arent, D. J.; Rubin, H. D.; Chen, Y.; Bocarsly, A. B. Cadmium Ferrocyanide Overlayers: Regulation of Photoinduced Charge Transfer at the *n*-CdSe/$[Fe(CN)_6]^{4-/3-}$ Interface. *J. Electrochem. Soc.* **1992**, *139*, 2705–2712.

43. Bicelli, L. P. Thermodynamic Stability of *n*-CdTe in Photoelectrochemical Cells. *J. Phys. Chem.* **1992**, *96*, 9995–10001.
44. Rajh, T.; Mićić, O. I.; Nozik, A. J. Synthesis and Characterization of Surface Modified Colloidal CdTe Quantum Dots. *J. Phys. Chem.* **1993**, *97*, 11999–12003.
45. Van de Walle, C. G.; Neugebauer, J. Universal Alignment of Hydrogen Levels in Semiconductors, Insulators, and Solutions. *Nature* **2003**, *423*, 626–628.
46. Gur, I.; Fromer, N. A.; Geier, M. L.; Alivisatos, A. P. Air-Stable All-Inorganic Nanocrystal Solar Cells Processed from Solution. *Science* **2005**, *310*, 462–464.
47. McGregor, S. M.; Dharmadasa, I. M.; Wadsworth, I.; Care, C. M. Growth of CdS and CdTe by Electrochemical Technique for Utilization in Thin Film Solar Cells. *Opt. Mater.* **1996**, *6*, 75–82.
48. Kampmann, A.; Lincot, D. Photoelectrochemical Study of Thin Film Semiconductor Heterostructures: Junction Formation Processes in CdS/CdTe Solar Cells. *J. Electroanal. Chem.* **1996**, *418*, 73–81.
49. Mathew, X.; Bansal, A.; Turner, J. A.; Dhere, R.; Mathews, N. R.; Sebastian, P. J. Photoelectrochemical Characterization of Surface Modified CdTe for Hydrogen Production. *J. New Mater. Electrochem. Syst.* **2002**, *5*, 149–154.
50. Guldi, D. M.; Zilberman, I.; Anderson, G.; Kotov, N. A.; Tagmatarchis, N.; Prato, M. Nanosized Inorganic/Organic Composites for Solar Energy Conversion. *J. Mater. Chem.* **2005**, *15*, 114–118.
51. Rogach, A. L.; Franzl, T.; Klar, T. A.; Feldmann, J.; Gaponik, N.; Lesnyak, V.; Shavel, A.; Eychmüller, A.; Rakovich, Y. P.; Donegan, J. F. Aqueous Synthesis of Thiol-Capped CdTe Nanocrystals: State-of-the-Art. *J. Phys. Chem. C* **2007**, *111*, 14628–14637.
52. Franzl, T.; Shavel, A.; Rogach, A. L.; Gaponik, N.; Klar, T. A.; Eychmüller, A.; Feldmann, J. High-Rate Unidirectional Energy Transfer in Directly Assembled CdTe Nanocrystal Bilayers. *Small* **2005**, *1*, 392–395.
53. Gross, D.; Susha, A. S.; Klar, T. A.; Da Como, E.; Rogach, A. L.; Feldmann, J. Charge Separation in Type II Tunneling Structures of Close-Packed CdTe and CdSe Nanocrystals. *Nano Lett.* **2008**, *8*, 1482–1485.
54. Cao, X. B.; Chen, P.; Guo, Y. Decoration of Textured ZnO Nanowires Array with CdTe Quantum Dots: Enhanced Light-Trapping Effect and Photogenerated Charge Separation. *J. Phys. Chem. C* **2008**, *112*, 20560–20566.
55. Yu, W. W.; Qu, L. H.; Guo, W. Z.; Peng, X. G. Experimental Determination of the Extinction Coefficient of CdTe, CdSe, and CdS Nanocrystals. *Chem. Mater.* **2003**, *15*, 2854–2860.
56. Yu, W. W.; Wang, Y. A.; Peng, X. G. Formation and Stability of Size-, Shape-, and Structure-Controlled CdTe Nanocrystals: Ligand Effects on Monomers and Nanocrystals. *Chem. Mater.* **2003**, *15*, 4300–4308.
57. James, D. R.; Liu, Y.-S.; de Mayo, P.; Ware, W. R. Distributions of Fluorescence Lifetimes: Consequences for the Photophysics of Molecules Adsorbed on Surfaces. *Chem. Phys. Lett.* **1985**, *120*, 460.
58. Ellis, A. B.; Kaiser, S. W.; Wrighton, M. S. Visible Light to Electrical Energy Conversion. Stable Cadmium Sulfide and Cadmium Selenide Photoelectrodes in Aqueous Electrolytes. *J. Am. Chem. Soc.* **1976**, *98*, 1635–1637.
59. Ellis, A. B.; Kaiser, S. W.; Wrighton, M. S. Optical to Electrical Energy Conversion. Characterization of Cadmium Sulfide and Cadmium Selenide Based Photoelectrochemical Cells. *J. Am. Chem. Soc.* **1976**, *98*, 6855–6866.
60. Lessner, P. M.; McLarnon, F. R.; Winnick, J.; Cairns, E. J. The Dependence of Aqueous Sulfur-Polysulfide Redox Potential on Electrolyte Composition and Temperature. *J. Electrochem. Soc.* **1993**, *140*, 1847–1849.
61. Ellis, A. B.; Kaiser, S. W.; Wrighton, M. S. Optical to Electrical Energy Conversion: Cadmium Telluride-Based Photoelectrochemical Cells Employing Telluride/Ditelluride Electrolytes. *J. Am. Chem. Soc.* **1976**, *98*, 6418–6420.
62. Peng, Z. A.; Peng, X. Formation of High-Quality CdTe, CdSe, and CdS Nanocrystals Using CdO as Precursor. *J. Am. Chem. Soc.* **2001**, *123*, 183–184.
63. Mann, J. R.; Watson, D. F. Adsorption of CdSe Nanoparticles to Thiolated TiO_2 Surfaces: Influence of Intralayer Disulfide Formation on CdSe Surface Coverage. *Langmuir* **2007**, *23*, 10924–10928.